

# Localized or itinerant $\text{TiO}_3$ electrons in $\text{RTiO}_3$ perovskites

H D Zhou<sup>1</sup> and J B Goodenough

Texas Materials Institute, ETC 9.102, 1 University Station, C2201, University of Texas at Austin, Austin, TX 78712-1063, USA

E-mail: [hdzhou@physics.utexas.edu](mailto:hdzhou@physics.utexas.edu)

Received 31 August 2005, in final form 4 October 2005

Published 1 November 2005

Online at [stacks.iop.org/JPhysCM/17/7395](http://stacks.iop.org/JPhysCM/17/7395)

## Abstract

A reinvestigation of nearly stoichiometric  $\text{RTiO}_3$  samples shows that (1) the transition from ferromagnetic to antiferromagnetic Ti–O–Ti interactions with increasing  $\text{R}^{3+}$ -ion radius  $r_{3+}$  occurs at  $r_{3+} \approx 1.11 \text{ \AA}$  where orthorhombic ( $Pbnm$ )  $\text{RMO}_3$  perovskites universally change structure from a cooperative rotation of undistorted to distorted  $\text{MO}_{6/2}$  octahedra about the orthorhombic  $b$ -axis, (2) the size of polaronic holes decreases progressively with  $r_{3+}$  from about ten Ti sites in  $\text{LaTiO}_3$  to small polarons in  $\text{GdTiO}_3$ , (3) the strength of the R–O–Ti interactions increases with the spin of the  $\text{R}^{3+}$  ion in the ferromagnetic compounds, (4) the saturation magnetization of the ferromagnetic  $\text{TiO}_3$  array at 5 K and the Curie temperature  $T_C$  both increase with decreasing  $r_{3+}$  where the  $\text{R}^{3+}$  ions have no spin, and (5) there is no evidence of ‘cluster-glass’ behaviour where there is no variance of the  $\text{R}^{3+}$ -ion radii. The cooperative Jahn–Teller orbital ordering and small-polaron behaviour of the ferrimagnetic and ferromagnetic compounds would favour localized Ti-3d electrons. However, the lack of saturation to  $1 \mu_B/\text{Ti}$  of the ferromagnetic  $\text{TiO}_3$  array in the absence of a spin on the  $\text{R}^{3+}$  ion suggests a separation of an orbitally ordered ferromagnetic phase and an orbitally disordered paramagnetic phase.

## 1. Introduction

All members of the  $\text{RTiO}_3$  perovskite family ( $\text{R} = \text{rare-earth or Y}$ ) have the Ti(IV)/Ti(III) and Ti(III)/Ti(II) redox couples separated by an energy gap that increases from 0.2 eV in antiferromagnetic  $\text{LaTiO}_3$  to near 1.2 eV in ferromagnetic  $\text{YTiO}_3$  [1–3]. The heavier rare-earth ions Gd–Yb all exhibit a ferromagnetic  $\text{TiO}_3$  array that couples antiparallel to a ferromagnetic component on the rare-earth array to give a net ferrimagnetism below a Curie temperature  $T_C$ ; the antiferromagnetic R–O–Ti interactions are reported to be weaker than the ferromagnetic Ti–O–Ti interactions [4, 5]. The lighter rare-earth ions Ce–Sm all have an antiferromagnetic

<sup>1</sup> Author to whom any correspondence should be addressed.

TiO<sub>3</sub> array like LaTiO<sub>3</sub> below a  $T_{N1}$  [6, 7]; the rare-earth moments order independently and antiferromagnetically below a  $T_{N2} < T_{N1}$ . The Curie temperature  $T_C$  decreases with decreasing atomic weight of the R<sup>3+</sup> ion from Dy to Gd, and  $T_{N1}$  increases from Sm to La [2, 8]. The long-range magnetic-ordering temperatures  $T_{N1}$  and  $T_C$  decrease to below 10 K at the crossover composition Sm<sub>0.5</sub>Gd<sub>0.5</sub>TiO<sub>3</sub> where there is no long-range orbital ordering [9].

The ferromagnetism of YTiO<sub>3</sub> below  $T_C \approx 30$  K is the result of G-type orbital ordering below a  $T_{OO} > T_C$  of the  $\pi$ -bonding  $t$  electron into a  $yz$  or  $zx$  orbital on alternate Ti(III) ions of the TiO<sub>3</sub> array [10]; the orbital ordering couples half-filled and empty  $\pi$ -bonding  $t$  orbitals on neighbouring Ti(III) ions to give ferromagnetic superexchange interactions in accordance with the Goodenough–Kanamori rules. However, at antiphase boundaries,  $yz$ – $yz$  or  $zx$ – $zx$  interactions between half-filled orbitals introduce an antiferromagnetic coupling across the boundary between ferromagnetic regions, which results in a low remanence [11].

The antiferromagnetic order of LaTiO<sub>3</sub> below a  $T_{N1} = 140$  K is due to a TiO<sub>6/2</sub> site deformation from cubic to rhombohedral symmetry that stabilizes an  $a_1$  orbital oriented along its [111] axis [12, 13]; moreover, the magnitude of the site deformation increases abruptly on cooling through  $T_{N1}$ . This orbital ordering has no preferred Ti–O–Ti axis and is, therefore, responsible for the G-type antiferromagnetic order found for the lighter R<sup>3+</sup> ions. Cwik *et al* [12] also observed that both the magnitude of the site deformation and  $T_{N1}$  decrease with the size of the R<sup>3+</sup> ion in the RTiO<sub>3</sub> family; the site deformation, but not its cooperative rotation about the orthorhombic ( $Pbnm$ )  $b$ -axis, essentially disappears in the ferromagnetic compositions having a G-type ordering of the occupied  $yz$  and  $zx$  orbitals. However, left unresolved is whether orbital order drives the site deformation or the site deformation stabilizes the orbital order.

Here we report a reinvestigation of nearly stoichiometric samples of the RTiO<sub>3</sub> family to determine (1) the origin of the site deformations, (2) the evolution with R<sup>3+</sup>-ion radius  $r_{3+}$  of the activation energy of polaronic p-type transport in the TiO<sub>3</sub> array, (3) how the strength of the R<sup>3+</sup>–O–Ti<sup>3+</sup> spin–spin interaction changes with the spin of the R<sup>3+</sup> ion in the ferromagnetic compositions, (4) how the saturation magnetization of the TiO<sub>3</sub> array approaches the spin-only value of  $1 \mu_B/\text{Ti}$  in the absence of a moment on the rare-earth ion, and (5) whether the report by Yoshii *et al* [14] of ‘cluster-glass’ behaviour in the R<sub>1–x</sub>Nd<sub>x</sub>TiO<sub>3</sub> perovskites with R = Ce or Pr is found where there is no variance of the R<sup>3+</sup>-ion radius.

## 2. Experimental details

Polycrystalline samples of RTiO<sub>3</sub> (R = rare earth or Y) were prepared by solid-state reaction. Stoichiometric mixtures of R<sub>2</sub>O<sub>3</sub> or Pr<sub>6</sub>O<sub>11</sub> or Tb<sub>4</sub>O<sub>7</sub> and Ti<sub>2</sub>O<sub>3</sub> were ground together for each composition; the powders were cold-pressed into pellets, placed into a molybdenum crucible and put into a tube that was then evacuated to  $\sim 10^{-6}$  Torr before firing at 1620 °C for 12 h.

A Perkin-Elmer TGA-7 thermogravimetric analyser was used to determine the oxygen content of the samples from the weight gain due to an oxidation of the Ti(III) ions to Ti(IV) on heating to 1000 °C in air. For all samples, the excess oxygen was smaller than 0.4%; they were oxygen-stoichiometric within experimental error.

Powder x-ray diffraction (XRD) patterns were recorded with a Philips PW 1729 powder x-ray diffractometer equipped with a pyrolytic graphite monochromator and Cu K $\alpha$  radiation (1.54059 Å); Si was the internal standard. Data were collected in steps of 0.020° over the range  $20^\circ \leq \theta \leq 60^\circ$  with a count time of 20 s per step. Peak profiles for the XRD data were fitted with the program JADE. All samples were single-phase to XRD.

Magnetic susceptibility measurements were made with a Quantum Design dc SQUID magnetometer after cooling in zero field (ZFC) or after cooling in a measuring field (FC) of

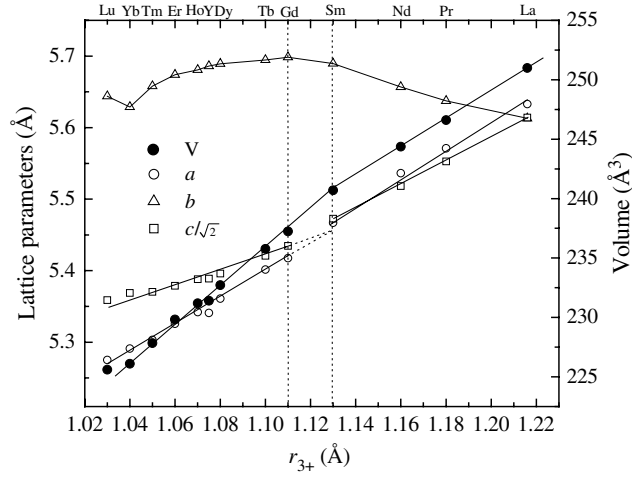


**Figure 1.** Variation with  $r_{3+}$  of the room-temperature lattice parameters of the orthorhombic  $Pbnm$  RTiO<sub>3</sub> perovskites. The dashed lines are guides for the eye.

100 Oe, 1 kOe, or 10 kOe.  $M$ – $H$  hysteresis loops of magnetization  $M$  versus applied magnetic field  $H$  were measured over the range  $-5 \text{ T} \leq H \leq 5 \text{ T}$  at 5 K.

The low-temperature thermoelectric power  $\alpha(T)$  was obtained from 80 to 320 K with a laboratory-built apparatus as described elsewhere [15]. The resistivity was measured by a four-probe technique on samples that were cold-pressed as mixed powders. The cold-pressing technique has been described elsewhere [16].

### 3. Results

All samples of the orthorhombic  $Pbnm$  perovskite family RTiO<sub>3</sub> were single-phase to XRD. Figure 1 displays the room-temperature variation of unit-cell volumes and lattice parameters with the  $R^{3+}$ -ion radius  $r_{3+}$  as calculated for ninefold oxygen coordination. The lattice parameters also are listed in table 1. The lattice parameter  $b$  increases with increasing  $r_{3+}$  to GdTiO<sub>3</sub>, where  $r_{3+} = 1.11 \text{ \AA}$ ; it decreases with a further increase in  $r_{3+}$  where  $c/a < \sqrt{2}$  is found.

All the RTiO<sub>3</sub> samples were p-type semiconductors with a  $\rho(T) \sim \exp(E_a/kT)$ , where  $E_a = \Delta H_m + (\Delta H_t/2)$  is the sum of the motional enthalpy and an enthalpy  $\Delta H_t$  of trapping at the cation vacancy that created the mobile holes. Figure 2 shows that an  $E_a \geq 0.23 \text{ eV}$  increases little with decreasing  $r_{3+}$  on passing from GdTiO<sub>3</sub> to LuTiO<sub>3</sub> whereas  $E_a$  increases sharply with decreasing  $r_{3+}$  on passing from LaTiO<sub>3</sub> with  $E_a = 0.035 \text{ eV}$  to GdTiO<sub>3</sub>. From thermoelectric-power measurements  $\alpha(T)$ , we have shown that the mobile holes in LaTiO<sub>3</sub> occupy itinerant-electron clusters containing multiple Ti atoms [11], and the data of figure 2 are consistent with a cluster size that decreases progressively to that of a small polaron as  $r_{3+}$  decreases. However, the high resistance of the samples with smaller  $r_{3+}$  did not permit a good measure of  $\alpha(T)$ , so we were unable to determine reliably the separate contributions of  $\Delta H_m$  and  $\Delta H_t$  for samples other than LaTiO<sub>3</sub> and therefore their separate evolutions with  $r_{3+}$ .

The magnetic susceptibilities  $1/\chi_m(T)$  and  $\chi_m(T)$  for  $R = \text{La, Pr, Nd, and Sm}$  are shown in figures 3 and 4; data were taken on heating after cooling in zero field (ZFC) and in the measuring field (FC) of  $H = 100 \text{ Oe, 1 kOe, or 10 kOe}$ . All samples show a  $T_{N1}$  that

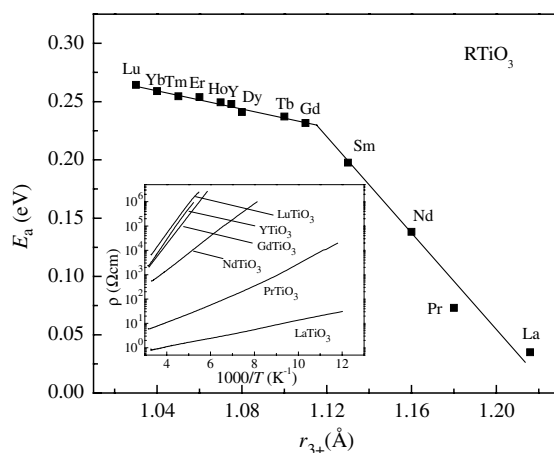


**Figure 2.** Variation with  $r_{3+}$  of the activation energy  $E_a$  of the resistivity  $\rho(T) \sim \exp(E_a/kT)$  for the p-type  $\text{RTiO}_3$  perovskites. Inset:  $\rho \sim 1/T$  curves for several  $\text{RTiO}_3$  samples. The straight lines are guides for the eye.

**Table 1.** Variation with R in  $\text{RTiO}_3$  of room-temperature lattice parameters.

$\text{RTiO}_3$	$a$ (Å)	$b$ (Å)	$c$ (Å)	$V$ (Å <sup>3</sup> )
La	5.633(1)	5.613(2)	7.942(2)	251.1
Pr	5.555(2)	5.615(1)	7.821(2)	244.0
Nd	5.524(1)	5.657(1)	7.795(1)	243.6
Sm	5.467(1)	5.669(1)	7.742(1)	240.0
Gd	5.402(2)	5.697(2)	7.680(2)	236.4
Tb	5.384(1)	5.678(1)	7.660(1)	234.2
Dy	5.363(3)	5.689(2)	7.647(1)	233.3
Y	5.341(1)	5.686(2)	7.621(1)	231.4
Ho	5.340(2)	5.689(2)	7.622(1)	231.5
Er	5.320(3)	5.674(3)	7.609(2)	229.7
Tm	5.303(1)	5.658(1)	7.597(3)	228.0
Yb	5.291(1)	5.629(1)	7.595(1)	226.0
Lu	5.275(1)	5.644(1)	7.581(2)	225.7

decreases progressively from 140 K in  $\text{LaTiO}_3$  to about 120 K in  $\text{PrTiO}_3$ , 110 K in  $\text{NdTiO}_3$ , and 70 K in  $\text{SmTiO}_3$  as determined by a divergence of the FC and ZFC curves below  $T_{N1}$  in  $H = 100$  Oe. This divergence is caused by a weak ferromagnetic component due to an antisymmetric exchange contribution  $D_{ij} \cdot S_i \times S_j$  with  $D_{ij}$  parallel to the  $b$  axis, which is associated with a canting of the antiferromagnetically coupled spins of the  $\text{TiO}_3$  array.

Where the  $\text{R}^{3+}$  ions have a large moment, these moments dominate the  $1/\chi_m(T)$  curves. Nevertheless, a deviation from Curie–Weiss behaviour below a  $T_1$  is found for all the heavier  $\text{R}^{3+}$  ions, figure 5; for these compounds,  $T_1$  decreases systematically with decreasing  $r_{3+}$  whereas  $T_C$  varies irregularly with  $r_{3+}$ , figure 6. Magnetic parameters are listed in table 2.

Figure 8 shows the  $M$ – $H$  hysteresis loops taken at 5 K for the heavier  $\text{R}^{3+}$  ions.

#### 4. Discussion

In figure 1, the linear increase of  $a$  and  $c$  and the decrease in  $c/a > \sqrt{2}$  with increasing  $r_{3+} < 1.11$  Å are consistent with a cooperative rotation of the  $\text{TiO}_{6/2}$  octahedra about

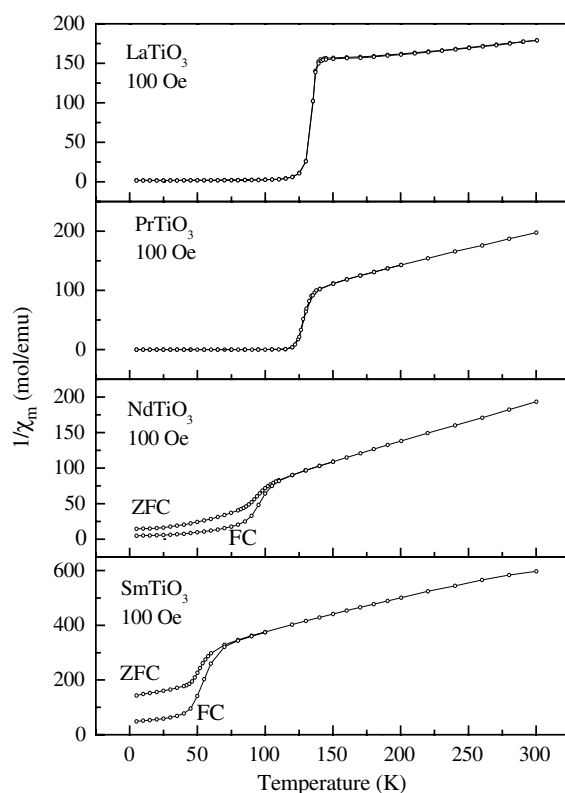


**Figure 3.** Inverse molar magnetic susceptibility  $1/\chi_m$  taken in  $H = 100$  Oe for RTiO<sub>3</sub> with R = La, Pr, Nd, and Sm.

**Table 2.** Variation with R in RTiO<sub>3</sub> of magnetic parameters.

RTiO <sub>3</sub>	$T_{N1}$ (K)	$T_{N2}$ (K)	$T_C$ (K)	$T_1$ (K)
La	140			
Pr	120	82		
Nd	110	80		
Sm	70	45		
Gd			32	179
Tb			49	170
Dy			60	150
Y			30	
Ho			56	135
Er			42	120
Tm			68	100
Yb			36	80
Lu			40	

the orthorhombic  $b$  axis that decreases in magnitude with increasing  $r_{3+}$ . The transition at  $r_{3+} \approx 1.11$  Å is similar to that found by Marezio [17, 18] in the RFeO<sub>3</sub> family and has been interpreted [19] to be due to a distortion of the MO<sub>6/2</sub> octahedra that is superimposed on the cooperative site rotations as a result of R–O interactions that occur where an  $r_{3+} > 1.11$  Å

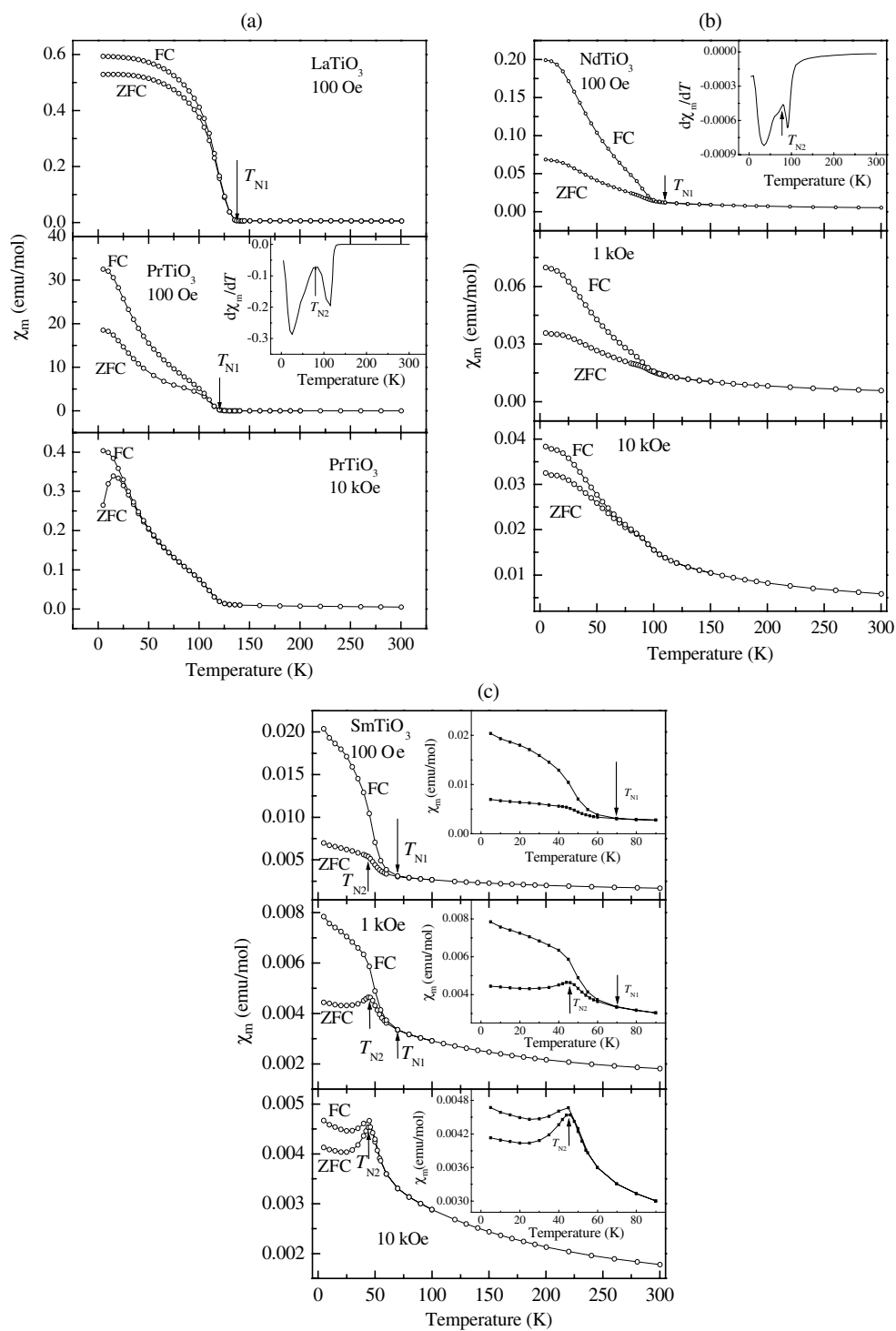


**Figure 4.** Molar magnetic susceptibility  $\chi_m$  for (a)  $\text{LaTiO}_3$  with  $H = 100$  Oe,  $\text{PrTiO}_3$  with  $H = 100$  Oe, 10 kOe; (b)  $\text{NdTiO}_3$  and (c)  $\text{SmTiO}_3$  with  $H = 100$  Oe, 1 kOe, and 10 kOe. Inset of (a) and (b): derivative of  $\chi_m(T)$  for  $\text{PrTiO}_3$  and  $\text{NdTiO}_3$ .

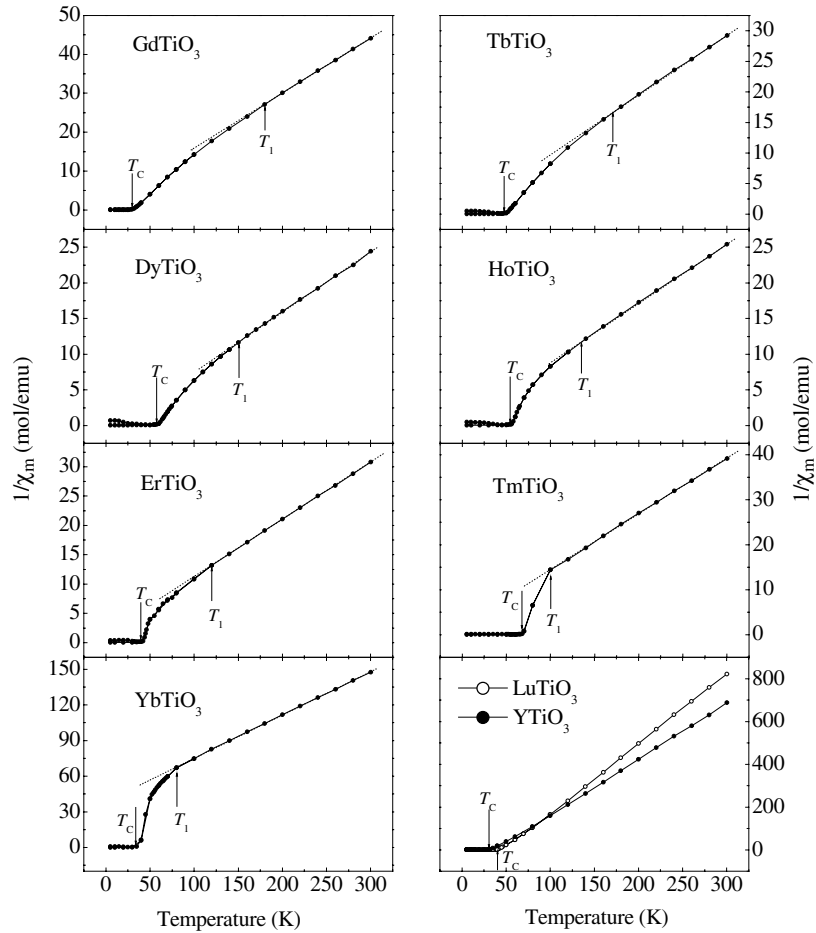


**Figure 5.** Inverse molar magnetic susceptibility  $1/\chi_m$  for RTiO<sub>3</sub> (R = Gd–Lu, Y), taken in  $H = 100$  Oe. The dashed lines are guides to the eye.

is found. This interpretation is consistent with the observation of Cwik *et al* [12] for the TiO<sub>3</sub> family. Accordingly, figure 1 shows that the unit-cell volume varies linearly with  $r_{3+}$  in accordance with Végard's law only in the region  $r_{3+} < 1.13$  Å where  $c/a > \sqrt{2}$  is found; for larger  $r_{3+}$ , a  $c/a \leq \sqrt{2}$  signals that a TiO<sub>6/2</sub> octahedral-site deformation is superimposed on the rotation, and this deformation results in smaller volumes  $V$  for R = Nd, Pr, and La than is predicted by extrapolation of  $V$  versus  $r_{3+}$  from compounds with a smaller  $r_{3+}$ .

Since the site deformation has been found to be a general property of RMO<sub>3</sub> perovskites with  $r_{3+} > 1.11$  Å where there is no orbital order, we may conclude that the site deformation is not driven by the orbital order; it is driven by the R<sup>3+</sup>–O interactions caused by shortening of an R–O bond length in the RO rock-salt (001) planes by the octahedral-site rotation. The site deformations stabilize, in turn, an orbital ordering of the single d electron of a Ti atom into an  $a_1$  orbital oriented along a site [111] axis, and the orbital order increases the magnitude of the site deformation. The strongly correlated electrons introduce a localized spin on the Ti<sup>3+</sup> ions; antiferromagnetic  $a_1^1$ –O– $a_1^1$  interactions between half-filled  $a_1$  orbitals below  $T_{N1}$  introduce an exchange striction that stabilizes further the orbital order, thereby enhancing the

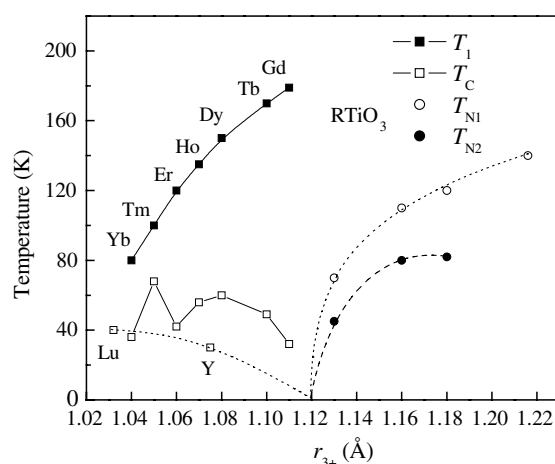


**Figure 6.** Transition temperatures  $T_1$ ,  $T_C$ ,  $T_{N1}$  and  $T_{N2}$  versus  $r_{3+}$  for  $\text{RTiO}_3$ . The dotted line is a guide to the eye of the Curie temperature for the  $\text{RTiO}_3$  compounds without any moment on the  $\text{R}^{3+}$  ion, i.e.  $\text{R} = \text{Lu}$  and  $\text{Y}$ . The curve is extrapolated to zero at  $\text{Sm}_{0.5}\text{Gd}_{0.5}\text{TiO}_3$  where there is a crossover from ferromagnetic to antiferromagnetic coupling within the  $\text{TiO}_3$  array.

site deformation. However, as the initial site deformation is reduced by introduction of a smaller  $\text{R}^{3+}$  ion, stabilization of the  $a_1^1$  configuration is more difficult, and  $T_{N1}$  decreases. Where the initial site deformation becomes negligible, the orbital order in the  $\text{TiO}_3$  array is stabilized by a cooperative Jahn–Teller distortion that minimizes the elastic energy and maximizes the ferromagnetic interactions. Cooperative Jahn–Teller distortions are a characteristic of localized electrons, and their orbital-ordering temperature increases (not shown in figure 6) as the bandwidth of the  $\text{Ti}^{4+}/\text{Ti}^{3+}$  redox couple narrows.

The activation energies  $E_a$  of figure 2 for the smaller  $\text{R}^{3+}$  ions ( $\text{R} = \text{Gd–Lu}, \text{Y}$ ) are typical for small-polaron conduction; those for the larger  $\text{R}^{3+}$  ions become increasingly smaller from  $\text{Sm}$  to  $\text{La}$ . As the transitions from strong to weak electron correlations in a single-valent parent compound is approached from the strong-correlation side, holes introduced into the occupied redox couple (lower Hubbard band) may not be confined to a single cation site, i.e. be self-trapped as a small dielectric polaron. For example, holes introduced into antiferromagnetic  $\text{La}_2\text{CuO}_4$  either by  $\text{Sr}$  substitution for  $\text{La}$  or by the introduction of interstitial oxide ions form polarons occupying five to six  $\text{Cu}$  centres in a  $\text{CuO}_2$  plane [20, 21]. These larger polarons have a smaller motional enthalpy because the oxygen displacements that define the polaron are smaller where the hole population per cation centre within the polaron is reduced [22]. Similarly, stoichiometric  $\text{LaTiO}_3$  is close to the transition from strong to weak electron correlations, i.e. to the Mott–Hubbard transition, and we have interpreted thermoelectric-power data for p-type  $\text{LaTiO}_3$  to reflect polaronic conduction with a polaron size approaching ten  $\text{Ti}$  centres in a 3D matrix [11]. The activation energy  $E_a$  for hole transport in  $\text{LaTiO}_3$  is, therefore, small. In the  $\text{RTiO}_3$  family, the bandwidth of the  $\text{RTiO}_3$  couple decreases with decreasing  $r_{3+}$ , which should reduce the size of the polaron until, below a critical value of  $r_{3+}$ , it occupies only a single  $\text{Ti}$  site, i.e. is reduced to a small polaron. As the size of a polaron shrinks, the oxygen displacements that define it become larger, which increases the motional enthalpy  $\Delta H_m$ . Once the size of the charge carriers is reduced to that of a small polaron, no further reduction in size can occur. Nevertheless, as the bandwidth of the redox energy decreases further, the electron localization becomes greater and  $E_a$  continues to increase, but less dramatically. From

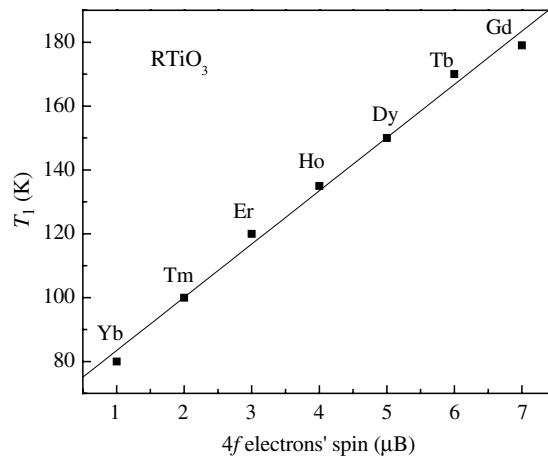


Figure 7. Variation of  $T_1$  with the  $R^{3+}$ -ion spin.

these considerations, we interpret figure 2 to signal a reduction of the polaron size from that found in LaTiO<sub>3</sub> to that of a small polaron as  $r_{3+}$  decreases between LaTiO<sub>3</sub> and GdTiO<sub>3</sub>. The narrowing of the redox bands is also manifest in an increase in the  $(U - W)$  energy gap between the  $Ti^{4+}/Ti^{3+}$  and  $Ti^{3+}/Ti^{2+}$  couples (the lower and upper Hubbard bands) from 0.2 eV in LaTiO<sub>3</sub> to 1.2 eV in YTiO<sub>3</sub> [1, 2].

The  $1/\chi_m(T)$  curve for LaTiO<sub>3</sub>, figure 3, shows a Weiss constant with an anomalously large magnitude ( $\theta = -853$  K) as well as too large a  $\mu_{\text{eff}} = 2.43 \mu_B$  for normal localized-electron behaviour; it has been accounted for by invoking orbital fluctuations [23], but it is also characteristic of itinerant-electron magnetism at the crossover to strongly correlated electrons. Below  $T_{N1}$ , the spins of the TiO<sub>3</sub> array order antiferromagnetically, but spin canting introduces a weak ferromagnetic component.

The large moments of the  $R^{3+}$  ions dominate the  $1/\chi_m(T)$  curves for  $R = \text{Pr, Nd, and Sm}$ . Below  $T_{N1}$ , only the weak ferromagnetic component of the TiO<sub>3</sub> array introduces an R–O–Ti interaction, and the R–O–R interactions are stronger. Therefore, the rare-earth ions order antiferromagnetically below a  $T_{N2} < T_{N1}$  [4, 5] where they introduce an additional canted-spin ferromagnetic component that couples to that of the TiO<sub>3</sub> array [24]. From the peak in the  $d\chi_m(T)/dT$  curve, see the inset of figure 4, we determine a  $T_{N2} = 82, 80,$  and  $45$  K for  $R = \text{Pr, Nd, and Sm}$ , respectively. The larger divergence of the FC and ZFC  $\chi_m(T)$  curves below  $T_{N2}$  reflects the large crystalline anisotropy of the  $R^{3+}$ -ion ferromagnetic component and its coupling to the ferromagnetic component of the TiO<sub>3</sub> array.

The R–O–Ti interactions are stronger than the R–O–R interactions where the TiO<sub>3</sub> array orders ferromagnetically, and an antiferromagnetic R–O–Ti interaction gives ferrimagnetic order below  $T_C$  [5]. Nevertheless, the  $1/\chi_m(T)$  curves for the heavier rare earths, figure 5, show a deviation from Curie–Weiss behaviour only below a  $T_1 > T_C$  that decreases smoothly with  $r_{3+}$ , figure 6. Figure 7 shows that  $T_1$  decreases linearly with the spin on the  $R^{3+}$  ion. Therefore, we conclude that  $T_1$  represents the onset of spin–spin coupling between the  $R^{3+}$  and  $Ti^{3+}$  ions in the paramagnetic phase. Figure 6 also shows that the coupling between the  $R^{3+}$  and  $Ti^{3+}$  spins tends to raise  $T_C$  above the value it would have were there no rare-earth spin, as is the case for  $R = \text{Lu and Y}$ . In addition, the larger  $T_C$  for LuTiO<sub>3</sub> than for YTiO<sub>3</sub> means that  $T_C$  increases as the bandwidth narrows, which is characteristic of itinerant-electron magnetism rather than of spin–spin interactions between localized-electron spins that are well

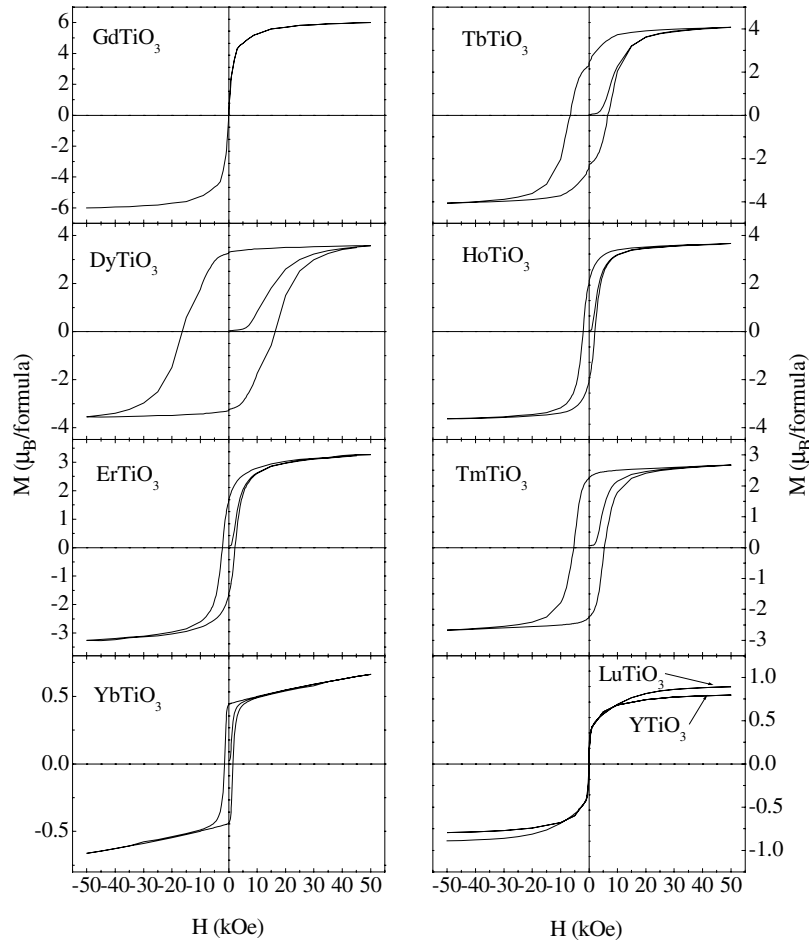


Figure 8.  $M$ - $H$  hysteresis loops taken at 5 K for  $\text{RTiO}_3$  ( $R = \text{Gd-Lu, Y}$ ).

described by perturbation theory. Therefore, we turn finally to the magnitudes of the saturation magnetization to see whether  $\text{LuTiO}_3$  has a ferromagnetic magnetization at  $T = 5$  K that is closer to the spin-only value of  $1 \mu_{\text{B}}/\text{Ti}$ .

The  $M$ - $H$  hysteresis loops of figure 8 show that at 5 K the saturation magnetization of  $\text{LuTiO}_3$  reaches  $0.9 \mu_{\text{B}}/\text{Ti}$  whereas that of  $\text{YTiO}_3$  is only  $0.8 \mu_{\text{B}}/\text{Ti}$ . On the other hand, an  $M_s(5 \text{ K}) = 6 \mu_{\text{B}}/\text{Ti}$  for  $\text{GdTiO}_3$  corresponds to full spin-only ferrimagnetism; the Gd-O-Ti interaction both raises  $T_{\text{C}}$  and fully magnetizes the  $\text{TiO}_3$  array. There is no evidence of an orbital contribution that lowers the magnetization of the  $\text{TiO}_3$  array. Moreover, the  $M$ - $H$  curves of the polycrystalline samples show no evidence of a large magnetocrystalline anisotropy. We are thus led to the conclusion that where there is no moment of the  $\text{R}^{3+}$  ion, the Ti-O-Ti spin-spin interaction of the strongly correlated electrons of the insulating, ferromagnetic  $\text{TiO}_3$  array is not strong enough to remove completely the spin degeneracy of the Ti-3d electrons.

Also noteworthy in figure 8 are the small remanences and coercivities of  $\text{GdTiO}_3$ ,  $\text{YTiO}_3$ , and  $\text{LuTiO}_3$ . As pointed out elsewhere [11], the G-type  $yz$ ,  $zx$  orbital ordering of the ferromagnetic  $\text{TiO}_3$  array is interrupted by antiphase boundaries across which the coupling is antiferromagnetic. Therefore, ferromagnetic blocks couple antiferromagnetically across these

boundaries in zero applied magnetic field, but a modest applied field exerts a high enough torque to align the blocks ferromagnetically provided there is no large magnetocrystalline anisotropy; the magnetocrystalline anisotropy associated with the R<sup>3+</sup> ion and the R–O–Ti coupling inhibits rotation to give a large  $M$ – $H$  hysteresis loop.

We found no evidence of ‘cluster-glass’ behaviour in any of our samples.

## 5. Conclusion

The orthorhombic ( $Pbnm$ ) structure of the RMO<sub>3</sub> perovskites can be described by a cooperative rotation of the MO<sub>6/2</sub> octahedra about the  $b$ -axis if the R<sup>3+</sup> ion has an ionic radius  $r_{3+} < 1.11$  Å; but an R–O interaction for  $r_{3+} > 1.11$  Å creates, in addition, a deformation of the MO<sub>6/2</sub> site to rhombohedral symmetry. Therefore, the stabilization of electronic charge along a site [111] axis in the RTiO<sub>3</sub> perovskites with R = La to Sm is driven by the site deformation, not by a cooperative Jahn–Teller orbital ordering. Occupancy of the  $a_1$  orbitals is responsible for antiferromagnetic order on the TiO<sub>3</sub> array, and  $T_{N1}$  decreases as the site deformation responsible for preferential occupancy of an  $a_1$  orbital decreases. On the other hand, the heavier R<sup>3+</sup> ions and Y<sup>3+</sup> have an  $r_{3+} < 1.11$  Å, and in these RTiO<sub>3</sub> perovskites the Ti<sup>4+</sup>/Ti<sup>3+</sup> redox band is narrow enough to stabilize a cooperative Jahn–Teller orbital ordering; the G-type order of the occupied  $yz$  and  $zx$  orbitals introduces, as previously noted by others [10], ferromagnetic Ti–O–Ti interactions. Therefore, the change from antiferromagnetic to ferromagnetic order at an  $r_{3+} \approx 1.11$  Å signals that the site deformations that determine the magnetic order are driven by cooperative Jahn–Teller orbital ordering for  $r_{3+} < 1.11$  Å and by a structural site deformation for  $r_{3+} > 1.11$  Å.

Holes introduced by a small cation (probably R<sup>3+</sup>) deficiency are polaronic, but the size of the polarons progressively decrease with  $r_{3+}$  from roughly ten Ti atoms per hole in LaTiO<sub>3</sub> to small polarons as the bandwidth narrows to that of GdTiO<sub>3</sub>.

The R–O–Ti spin–spin coupling is stronger than the R–O–R coupling in the ferrimagnetic RTiO<sub>3</sub> compounds with  $r_{3+} < 1.11$  Å, but the R–O–R coupling is the stronger in the antiferromagnetic compounds having an  $r_{3+} > 1.11$  Å. In the ferrimagnetic compounds, the strength of the R–O–Ti interactions is proportional to the magnitude of the R<sup>3+</sup>-ion spin.

Although the electrons of the TiO<sub>3</sub> array are strongly correlated in all members of the RTiO<sub>3</sub> family, LaTiO<sub>3</sub> is close to the threshold for a transition to metallic behaviour and, in the absence of a spin on the R<sup>3+</sup> ion, the saturation magnetization at 5 K of a ferromagnetic TiO<sub>3</sub> array increases with decreasing bandwidth of the Hubbard bands. Therefore, we conclude that the abnormal magnetic behaviour of LaTiO<sub>3</sub> reflects an itinerant-electron antiferromagnetism of the strongly correlated electrons. The Jahn–Teller cooperative orbital ordering and the apparent small-polaron behaviour found for compounds with  $r_{3+} < 1.11$  Å would appear to signal localized-electron behaviour; the interatomic spin–spin interactions would then be described by a virtual charge transfer from a half-filled to an empty orbital in superexchange perturbation theory. However, in the absence of any evidence of a strong orbital magnetism or magnetocrystalline anisotropy of the TiO<sub>3</sub> array, the evidence for failure of the on-site electron–electron interactions to remove completely the spin degeneracy of the ferromagnetic Ti-3d electrons where there is no spin on the R<sup>3+</sup> ions either implies an incomplete orbital ordering as a result of a phase separation into an orbitally ordered phase and an orbitally disordered phase that decreases in volume fraction as the lower Hubbard band narrows or it poses a challenge to the theorist to develop a more adequate description of the evolution of magnetic properties from the onset of a strong-correlation energy gap to localized-electron ferromagnetism.

Finally, we found no evidence for ‘cluster-glass’ behaviour in our samples where there was no variance of the R<sup>3+</sup>-ion radius.

## Acknowledgments

The NSF and the Robert A Welch Foundation of Houston, TX, are thanked for financial support.

## References

- [1] Goral J P, Greedan J E and MacLean D A 1982 *J. Solid State Chem.* **43** 244
- [2] Okimoto Y, Katsufuji T, Okada Y, Arima T and Tokura Y 1995 *Phys. Rev. B* **51** 9581
- [3] Onoda M and Kohno M 1998 *J. Phys.: Condens. Matter* **10** 1003
- [4] Turner C W and Greedan J E 1980 *J. Solid State Chem.* **34** 207
- [5] Turner C W, Collins M F and Greedan J E 1981 *J. Magn. Magn. Mater.* **23** 265
- [6] Onoda M and Yasumoto M 1997 *J. Phys.: Condens. Matter* **9** 3861
- [7] Onoda M and Yasumoto M 1997 *J. Phys.: Condens. Matter* **9** 5623
- [8] Greedan J E 1985 *J. Less-Common Met.* **111** 335
- [9] Amow G, Zhou J S and Goodenough J B 2000 *J. Solid State Chem.* **154** 619
- [10] Itoh M, Tsuchiya M, Tanaka H and Motoya K 1999 *J. Phys. Soc. Japan* **68** 2783
- [11] Zhou H D and Goodenough J B 2005 *Phys. Rev. B* **71** 184431
- [12] Cwik M, Lorenz T, Baier J, Müller R, André G, Bourée F, Lichtenberg F, Freimuth A, Schmitz R, Müller-Hartmann E and Braden M 2003 *Phys. Rev. B* **68** 060401(R)
- [13] Eremina R M, Eremin M V, Iglamov V V, Hemberger J, Krug von Nidda H A, Lichtenberg F and Loidl A 2004 *Phys. Rev. B* **70** 224428
- [14] Yoshii K and Nakamura A 1998 *J. Solid State Chem.* **137** 181  
Yoshii K, Nakamura A, Abe H and Morii Y 2000 *J. Solid State Chem.* **153** 145  
Yoshii K, Nakamura A and Abe H 2000 *J. Alloys Compounds* **307** 25
- [15] Goodenough J B, Zhou J S and Chan J 1993 *Phys. Rev. B* **47** 5275
- [16] Zhou J S, Goodenough J B and Dabrowski B 2003 *Phys. Rev. B* **67** 020404(R)
- [17] Marezio M, Remeika J P and Dernier P D 1970 *Acta Crystallogr. B* **26** 2008
- [18] Marezio M and Dernier P D 1971 *Mater. Res. Bull.* **6** 23
- [19] Zhou J S, Goodenough J B and Dabrowski B 2004 *Phys. Rev. B* **70** 081102(R)
- [20] Zhou J S and Goodenough J B 1996 *Phys. Rev. B* **54** 12488
- [21] Goodenough J B 2003 *J. Phys.: Condens. Matter* **15** R257
- [22] Bersuker G I and Goodenough J B 1997 *Physica C* **274** 267
- [23] Khaliullin G 2005 *Phys. Rev. B* **64** 212405  
Kikoin K, Entin-Wohlmann O, Fleurov V and Aharony A 2003 *Phys. Rev. B* **67** 214418
- [24] Greedan J E 1984 *J. Magn. Magn. Mater.* **44** 299